Toward cell-inspired materials that feel: measurements and modeling of mechanotransduction in droplet-based, multi-membrane arrays

2016 Bioinspir. Biomim. 11 036008

(http://iopscience.iop.org/1748-3190/11/3/036008)

Bioinspiration & Biomimetics

PAPER

Toward cell-inspired materials that feel: measurements and modeling of mechanotransduction in droplet-based, multi-membrane arrays

Nima Tamaddoni and Stephen A Sarles

Department of Mechanical, Aerospace and Biomedical Engineering, University of Tennessee, Knoxville, 1512 Middle Dr, 414 Dougherty Engr. Bldg., Knoxville, TN, 37996, USA

E-mail: ssarles@utk.edu

RECEIVED
29 December 2015

REVISED
29 February 2016

ACCEPTED FOR PUBLICATION
22 March 2016

PUBLISHED
29 April 2016

Keywords: droplet interface bilayer (DIB), membrane based hair cell, multi-membrane serial droplet array, mechanotransduction, capacitive sensing, Helfrich membrane bending, Stoke's pendulum theory

Supplementary material for this article is available online

Abstract

The droplet interface bilayer (DIB) was recently used to show that a 5 nm thick lipid membrane placed near a vibrating synthetic hair could transduce hair motion into electrical current. Herein, we study for the first time mechanoelectrical transduction of hair motion using multi-membrane DIB arrays formed with more than 2 droplets connected in series, and we introduce a transduction model to investigate how airflow across the hair generates current in a membrane-based hair cell. Measurements of sensing currents across every membrane in serial chains of up to 5 connected droplets demonstrate that perturbation of a single hair creates vibrations that propagate across several droplets, allowing for membranes that are not directly attached to the hair to still transduce its motion. Membranes positioned closest to the hair generate the largest currents, while those farther away produce less current due to energy loss from fluid damping. Inserting multiple hairs of different lengths into different droplets in the array yields sensing currents that exhibit multiple characteristic frequencies in addition to location specific current intensities, features that can be used to spatially localize mechanical perturbations. We also develop a transduction model that provides an order-of-magnitude approximation of the sensing current generated by a membrane in response to airflow across the hair. This model provides physical insights into how membrane-based materials can be used for sensing mechanical stimuli—just like nature does.

1. Introduction

A distinct feature of the droplet interface bilayer (DIB) is its modular assembly procedure, which allows for multiple lipid-coated water droplets to be joined to construct networks of lipid bilayer membranes in two [6, 24, 29, 51] and three [16, 64–66] dimensions, where the bilayers regulate transport between the aqueous interiors of adjacent droplets. Multi-bilayer DIB arrays thus provide a unique platform for mimicking the compartmentalization and coordinated transport that are ubiquitous in living cells and tissues: to-date DIB networks have been employed to convert visible light into proton currents [24], demonstrate tissue-like actuation via osmosis [64], and enable circuit-like functionality using ion channels [29, 33].

The membrane-based, hair cell-inspired sensor [55, 61] was the first use of DIBs to convert a mechanical stimuli such as airflow into an electrical signal. Unlike other hair cell-inspired solid-state devices [15, 18, 30–32, 35, 36, 42–44, 48], this approach consists of a fluid lipid membrane arranged between two lipid-coated water droplets contained within an oil-filled polymeric substrate. This one-bilayer assembly allowed for experimentally studying the transduction mechanism, as well as exploring the sensor's sensitivity and directionality [61]. An artificial hair (i.e. cilium) inserted into one of the volumes mechanically couples motion of the hair to the bilayer membrane, which behaves as a deformable electrical capacitor. The vibration of the membrane causes a time rate of change of capacitance, dC/dt, that results in sensing

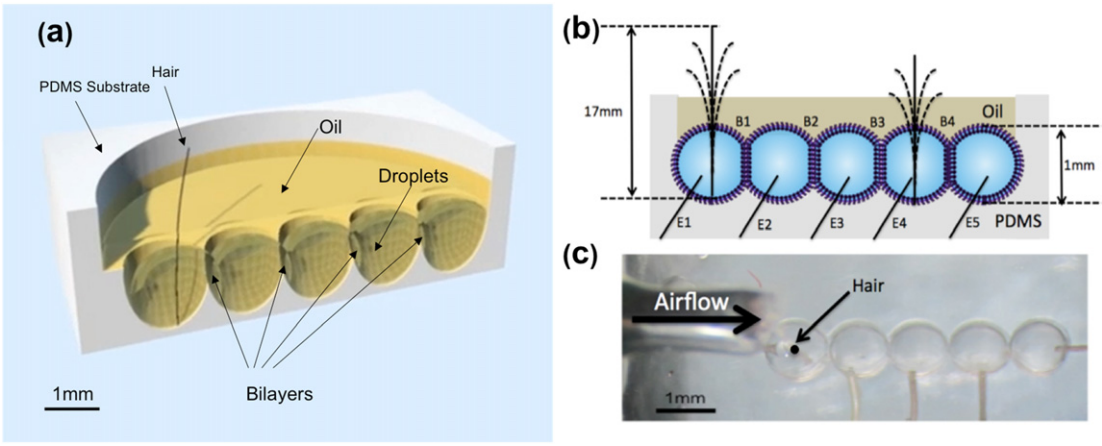

Figure 1. (a) Isometric view illustration of a multi-membrane, serial droplet array hair cell sensor. (b) Side view schematic of the 5-droplet series instrumented with wire-type electrodes. (c) A top view image of an assembled 5-droplet serial array. The hair (out of focus) is oriented vertically, extending out of the plane of the image.

current, i, given by:

$$i = \frac{dC}{dt}(V + \alpha V^3), \quad (1)$$

where, V is the voltage across the membrane, and α is an electrowetting constant that describes how the area, and therefore the capacitance of the membrane is affected by voltage.

A key functional difference between a natural hair cell, such as an outer hair cell in the organ of Corti [1, 12, 17, 25, 49], and a droplet-based membrane hair cell is that the synthetic version does not utilize membrane-bound ion channels to transduce membrane tension or affect membrane curvature in response to cilia motions [26, 27]. And while Najem, et al recently demonstrated dynamic mechanical activation of reconstituted mechanosensitive ion channels in a DIB [37, 38], a lipid-only membrane-based hair cell utilizes the mechanoelectrical response of the capacitive lipid membrane to convert mechanical vibration into current. Past works by our group determined the origin of this passive response [55] and quantified its sensitivity, dynamic range, and directionality [61] using a sensor embodiment that consisted of a hair and a single lipid bilayer formed between two droplets as the transduction element.

Yet, despite the unique capability of the DIB method for constructing multi-bilayer arrays, the mechanoelectrical sensing capability of multi-bilayer droplet networks has not been studied. We hypothesize that the vibration induced by hair motion can propagate through multiple droplets, thereby allowing bilayers formed between droplets that are not in direct contact with the hair to sense hair motion. By understanding both how mechanical forces affect the sensing current in a single interface and how these mechanical forces transmit in DIB arrays, we propose that in addition to compartmentalized biomimetic systems for regulated transport [6, 10, 21, 29, 60], actuation [7, 45, 57], and sensing [47, 53], DIB arrays can also be applied to the development of tissue-like materials systems for spatially distributed sensing of dynamic forces, fluid flow, and vibration—just like how spiders [3, 4], fish [19, 68], and mammals [11] use hair cells to perceive their surroundings.

In this paper, we study the mechanoelectrical responses of multi-membrane DIB arrays constructed from lipid-coated aqueous volumes connected in series and we demonstrate that, despite viscous energy dissipation between neighboring droplets, multiple interface bilayers in a DIB array are able to sense hair motion. We also present a physical transduction model that combines Stoke's theory for oscillatory hair motion, the Helfrich expression for membrane elasticity, and our own expression for capacitive current generation (equation (1)) to relate airflow to capacitive sensing current. Through both experiments and modeling, we demonstrate that multi-membrane serial DIB arrays provide a biomimetic method for sensing current in response to hair motion and enabling spatial recognition of multi-hair perturbation. The findings of this work provide insights into how droplets, membranes, and hairs can be effectively arranged for sensing and energy harvesting applications, as well as inducing mechanical stimulation necessary to excite transmembrane proteins like mechanosensitive channels [59].

2. Materials and methods

We assemble and characterize serial DIB array configurations that differ in the number and arrangement of droplets, bilayers, and hairs to examine how multiple membranes contribute to mechanotransduction of the hair's motion. Figure 1 shows a representative 5-droplet, 4-bilayer linear array that features a single hair positioned in the leftmost droplet of the series.

2.1. Assembly of droplet arrays

Flexible polydimethylsiloxane (PDMS) substrates are fabricated to support the hair(s) and contain the droplet arrays in oil (figure 1(a)). Substrates are made from Sylgard 184 PDMS (Dow Corning) via a double molding step as previously introduced [54, 55]. Based on the use of a manual micropipette for dispensing droplets that are ca. 1 mm in diameter, we use molding templates that contain up to five droplet compartments (each 1.016 mm diameter, 2 mm deep with hemispherical bottom surfaces) arranged in a collinear series (figure 1). The compartments are spaced relative to one another to provide a 0.3 mm wide dividing aperture in the PDMS substrates. Figure 1(b) shows how a 4-bilayer (B1–B4) array is supported in the substrate and instrumented for measurements. Silver–silver chloride (Ag/AgCl) wire-type electrodes (E1–E5) made from bleaching 125 μm diameter silver wire are inserted through the sides of the substrate such that the electrode tips pierce the lipid-coated droplets (figure 1(b)). Paintbrush fibers (80 μm in diameter) are inserted vertically into the PDMS in the center of the desired compartments. Hairs of two lengths are used in these experiments: one is 14 mm (free length, defined as the length of the hair not inserted into the substrate, of 11–13 mm) and the other is approximately 18 mm (free length of 15–17 mm). These hair dimensions allow for easy insertion through the center of 1 mm diameter droplets and provide a free length that is significantly taller than the droplets such that perturbations can be applied independently to the hair without affecting the oil or droplets. Figure 1(c) shows a top view image of a 5-droplet array, with an Ag/AgCl electrode in each of the droplets.

Hexadecane (99% Sigma Aldrich) is used as the immersing oil phase in all experiments. All droplets consist of a 2 mg ml^{-1} solution of 1,2-diphytanoyl-sn-glycero-3-phosphocholine (DPhPC, Avanti Polar Lipids, Inc.) unilamellar liposomes suspended in electrolyte containing 200 mM NaCl (Sigma Aldrich), 10 mM 3-(N-Morpholino) propanesulfonic acid (MOPS, Sigma Aldrich) and buffered to pH 7. Liposome solution is prepared as described elsewhere [60] and stored at 4 °C for use within two weeks.

The following procedure is performed to dispense, position, and attach lipid-coated droplets in a substrate after insertion of the hair: 50 μl of hexadecane is first dispensed into the vacant compartments in the substrate and then 750 nl of lipid solution is pipetted into each compartment. The droplets are incorporated in an order such that each droplet resides in oil for 3–5 min to allow for monolayer formation prior to being placed in contact with droplets in adjacent compartments. In the event of droplet coalesence, the volumes can be divided *in situ* by laterally compressing the solid substrate with a micromanipulator (SM-325, World Precision Instruments Inc.) as described elsewhere [54] for two-compartment substrates. The apertures are then reopened after 3–5 min by reducing compression on the substrate, whereby bilayers form spontaneously between every adjacent lipid-encased droplet.

2.2. Measurements of electrical sensing currents

Bilayer formation is confirmed and perturbation-induced sensing responses are characterized using current measurements via the Ag/AgCl electrodes contacting the droplets. The electrode from each compartment is connected to a separate measurement channel on a Triton eight-channel patch clamp amplifier (Tecella) such that voltage is independently applied to each droplet and the current entering or exiting each droplet is independently measured. Capacitance measurements are performed to verify the increase in membrane capacitance that occurs upon bilayer thinning [22]; these measurements are also used to estimate the area of each membrane using a specific capacitance of 0.65 μF cm^{-2} [51]. Specifically, the multi-channel amplifier is employed to record the resulting square-wave currents induced by a 100 mV, 5 Hz triangular voltage waveform designed in TecellaLab software and output by the same amplifier. The triangular voltage waveforms are removed after measuring the capacitances of all membranes in an array.

A dc voltage is applied across every membrane to characterize its sensing response to hair perturbation since capacitive current is voltage-dependent [55, 61]. In a serial array of droplets, one droplet is assigned as the 'virtual ground' for the circuit [51] and each lipid bilayer receives an identical transmembrane voltage (e.g. 40 mV) by assigning the voltage at the other electrodes to successive multiples of the same value. All current measurements are sampled at 20 kHz, low-pass filtered at 2 kHz within the amplifier, and saved as text files for analysis in MATLAB. All experiments are performed within a grounded, homemade Faraday cage.

2.3. Characterization of sensing responses

In this work we perturb hairs using two methods: (1) with a narrow horizontal stream of air at constant velocity across a portion of the free length of the hair, which causes the hair to vibrate, and (2) by bending and releasing the hair with a motorized 'flicker' that impacts the hair at a distance of 1–2 mm from the free end. As described previously [61], a narrow stream of air impacting the hair causes the hair to bounce in and out of the stream. Thus, analysis of the sensing currents generated by airflow induced vibration enables measurement of the root mean squared (rms) sensing response [55, 61] for each 10 s flow duration. Separately, sensing responses to hair flicking are used specifically to investigate the relative timing between sensing currents in multi-bilayer arrays. The subsequent hair motion caused by either source transfers vibration to the lipid bilayer, causing a time rate

change of capacitance in the membrane that generates current [55, 61]. The dc transmembrane voltage applied equally to all bilayers is varied from 0 to +100 mV, and measurements are performed multiple times at each voltage level and for each array configuration. Repeated flicking responses ($n > 10$) are assessed by computing the average net charge displaced across each bilayer—i.e. the area under the current–time trace—during ring-down. The displaced charge across a single bilayer for a single flick of the hair is ca. 2–20 pC mm^{-2} [61]. Before each sensing experiment, a control measurement is performed by flicking the hair rooted in the substrate containing only electrodes and oil (i.e., no droplets and bilayers) to quantify the charge displaced by electrode vibration —a feature that is independent of applied voltage [61]. These amounts of background current (or displaced charge) for each electrode are then removed from the measured responses when a vibrating membrane is present.

3. Results

3.1. Sensing responses in multi-bilayer serial droplet arrays

We first characterized the voltage-dependent sensing responses for membranes in a 5-droplet, 4-bilayer serial array that contained a single, 18 mm long hair positioned in the leftmost droplet. Figure 2(a) shows the resulting bilayer currents generated by all bilayers in response to a single flick of the hair in a direction parallel to the droplet series (i.e., perpendicular to the membranes) at a transmembrane potential of +40 mV. To help visualize this response, a slow-motion animation of the incurred motion of the hair and droplets in this multi-bilayer hair cell assembly is provided in video format in the ESI.

All four interfaces produce nearly synchronized, underdamped currents of about 100 pA or less that decay to the noise level within ca. 0.15 s (figure 2(a)). The first bilayer, at the perimeter of the droplet with the hair, generates the largest response, whereas the next three yield currents that are successively smaller in amplitude in response to the same flick. Integrating the sensing currents across the decay period and dividing each by their respective interfacial areas [61] allows for comparing the average responses of each successive interface in the series at a fixed voltage level; as shown in figure 2(b) bilayer 1 exhibits a net charge displacement of ca. 14.8 pC mm^{-2}, whereas bilayer 4 generates only 2–3 pC mm^{-2} in response to a single flick. The data points in this plot correspond to the displaced charge for each bilayer in a 5-droplet series averaged across identical measurements on three separate arrays; the response for each bilayer in a given array represents the average response to 10 hair flicks at +40 mV bias. The error bars represent ±1 standard deviation of displaced charge for the three separate arrays ($n = 3$). Similarly, figure 2(c) shows that the membrane closest to the hair (i.e., bilayer 1) produces the largest amplitude of current, while the interface farthest from the hair (i.e., bilayer 4) again produces the smallest response to airflow across the tip of the hair. Like with a single bilayer DIB [55, 61], these sensing currents are functions of the third power of voltage as described by equation (1). Furthermore, plotting the power spectral density (PSD) of each current signal computed using Welch's method in MATLAB (not shown) confirms that all membranes vibrate at the same frequency (158 Hz), which we have previously proven to correspond to the first natural bending frequency of the cantilevered hair [61].

Equation (1) specifies that measuring sensing currents across each of the four membranes at varying voltages (+20, +40, +60, +80, and +100 were used here) can be used to estimate the time rate change in capacitance of each interface in the array. Using this approach, we determine values of dC/dt from rms current measurements for all four membranes in the array for three airflow speeds across the hair. Figure 2(d) shows that, like the raw current traces, the time rate change in capacitance decreases with distance away from the hair. Here, the data points and error bars represent the average dC/dt (and % area change) ±1 standard deviation, respectively, for each bilayer determined from measurements at 5 different transmembrane voltages (required for computing dC/dt) and averaged across $n = 3$ separate 5-droplet arrays. Tests were performed identically at 3 different airflow speeds. Consistent with single membranes [61], we also observe that faster airflow yields higher values of dC/dt (left axis) for all bilayers, corresponding to higher percentage changes in membrane area (right axis) [61]. For example, the bilayer closest to the hair exhibits a dC/dt of approximately 4.5 nF s^{-1} and a maximum change in membrane area of approximately 1.3% when airflow at 13.5 m s^{-1} is applied to the hair, compared to ca. 2.9 nF s^{-1} and 0.7%, respectively, for airflow at 10.7 m s^{-1}.

As a result, these data demonstrate that multiple membranes in a droplet array are capable of performing mechanoelectrical transduction of hair motion via membrane bending. The magnitudes of current response, as expected, show that membranes closer to the moving hair result in larger capacitive currents due to greater amounts of bending, whereas membranes farther away generate smaller responses. The observed decay in sensing response is due to the viscous damping in the system that dissipates the strength of the propagating pressure front originating in the liquid from the moving hair. Exponential fits to find the decay rates of displaced charge in figure 2(b) or dC/dt in figure 2(d) show that the decay rate is independent of the voltage and stimuli strength. The decay rate of displaced charge induced by flicking at three different transmembrane voltages is −0.59 ± 0.13 pC mm^{-2} per bilayer. Moreover, the average decay rate for airflow-induced dC/dt

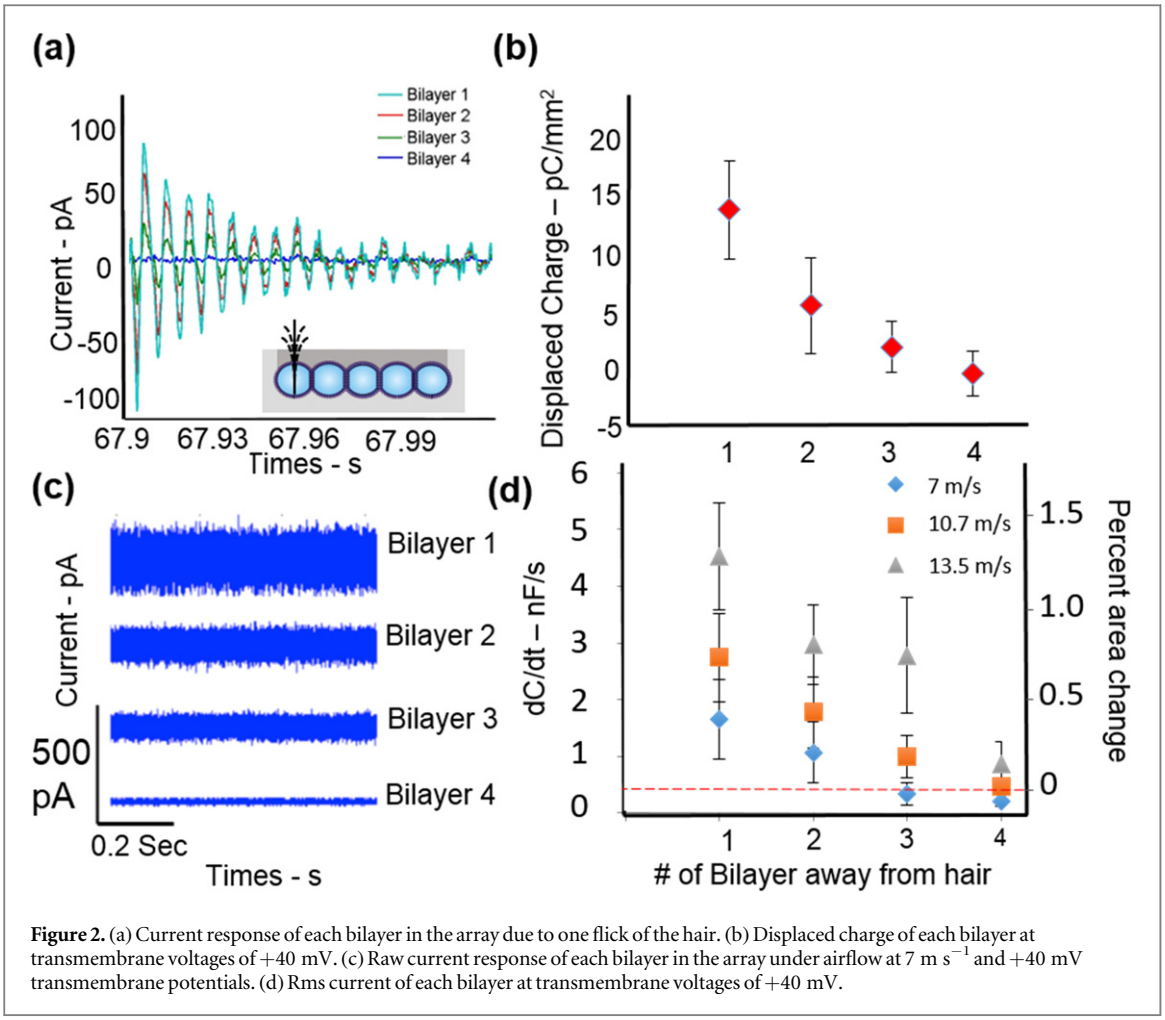

Figure 2. (a) Current response of each bilayer in the array due to one flick of the hair. (b) Displaced charge of each bilayer at transmembrane voltages of +40 mV. (c) Raw current response of each bilayer in the array under airflow at 7 m s^{-1} and +40 mV transmembrane potentials. (d) Rms current of each bilayer at transmembrane voltages of +40 mV.

at three different air speeds is found to be -0.36 ± 0.06 nF s^{-1} per bilayer.

The data also specifically show that the maximum distance a membrane can be located away from the hair and still elicit a measureable sensing response depends in part on the amplitude of the mechanical input that drives hair motion. In these experiments, the motion of the hair resulted in measurable sensing currents up to the 4th bilayer in the series. As is shown in figure 2(d), the measured values of dC/dt at 7 and 10.7 m s^{-1} airflow speeds are barely detectable above the baseline level determined in control experiments with no airflow. Therefore, bilayers that would be located farther away in a longer droplet series are likely insensitive to hair motion in the current sensor embodiment.

Not surprisingly, the membrane positioned closest to the hair was also consistently the first to rupture in the array upon further increases in airflow speed. We found this response is a function of both the applied airflow speed and the applied voltage level. For example, in separate experiments the membrane closest to the hair ruptured when we applied |120 mV| at 7 m s^{-1} airflow, |100 mV| at 10.7 m s^{-1} airflow, and |80 mV| at 13.5 m s^{-1}, respectively. These boundaries indicate that both the dynamic range of operation and the minimum sensing threshold are tied to the ability to transmit and withstand mechanical vibration along the droplet series.

To compare the total displaced charge in response to hair flicking produced by a single-DIB membrane sensor versus those obtained here with a multi-bilayer hair cell, we plot the total displaced charges in an asymmetric four-droplet, three-membrane hair cell sensor array versus that for a single membrane sensor (figure S1 in the supporting information (SI)). This result shows that the response generated by the one-hair, three-membrane sensor is considerably larger than that of a one-hair, single bilayer sensor. We are also interested to compare the sensing response generated by an equal number of bilayers arranged in separate single-DIB hair cell sensors to the total output from the four-droplet, three-membrane serial array. Figure S1 reveals that a four-droplet, three-interface serial array produces a similar magnitude of displaced charge to that estimated for three separate single-bilayer hair cells sensors.

3.2. Phase of the sensing currents with respect to hair motion

In addition to understanding the magnitudes of sensing response by adjacent bilayers, we seek to

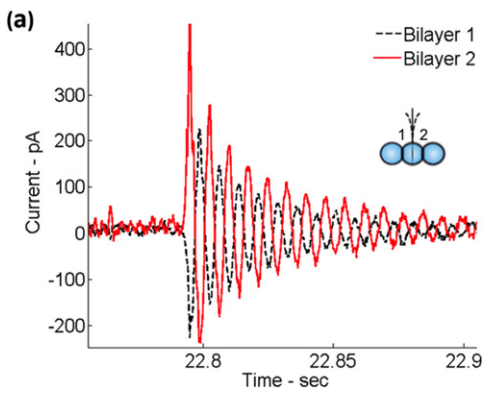

(b)

		Bilayer 1 V= 40mV	Bilayer 2 V= 40mV	Bilayer 3 V= 40mV
Asymmetric	Relative Phase Lag	ϴ°	ϴ+8.1°	ϴ+16.2°
	Bending membranes	In phase	In phase	In phase
Symmetric	Relative Phase Lag	ϴ	ϴ+180+6.1°	
	Bending membranes	Out of phase	Out of phase	

Figure 3. (a) Measured sensing currents of both bilayers in a three-droplet array in response to flicking a hair positioned in the middle droplet. (b) Table of phase analysis of sensing currents and membrane bending in asymmetric and symmetric serial arrays.

understand how hair placement in an array affects the relative timing, or phase angle, of bilayer currents. Figure 3(a) shows the transient bilayer currents recorded at equal transmembrane potentials of +40 mV for all bilayers in a *symmetric* three-droplet, two-bilayer array when a hair placed in the central droplet is flicked. This response is compared to that of the first 3 membranes (counted left to right) in the 5-droplet, 4-bilayer array with a single hair inserted into the leftmost droplet shown in figure 1(a)—referred to in this section as the *asymmetric* array due to the asymmetric position of the hair. We observe that for both series hair motion induces a current response at every membrane. This result shows that bilayers positioned on the same side of the excited droplet (figure 1(a)) or symmetrically on both sides of the excited droplet (figure 3(a)) transduce vibrational energy from the hair with the amplitude being a function of distance from the hair. The slight differences in the amplitudes of current produced by both adjacent membranes in the symmetric array may be due to differences in their areas or because of variations in membrane orientation relative to the motion of the hair [52].

The more apparent difference between the transient responses of these droplet arrays is that the sensing currents for the asymmetric three-bilayer array appear to occur in synchronization, while the measured currents for the two bilayers positioned symmetrically on opposite sides of the hair are out-of-phase with each other (figure 3(a)). We performed cross-correlation analyzes of these signals using MATLAB to quantify the time delays between sensing currents of adjacent membranes in both systems. The coefficients versus lag times for cross-correlations performed between membrane currents for both the 2 bilayers of the symmetric array and the 3 membranes of the asymmetric array are plotted in figure S2 in the SI. The delay time between current responses is determined by locating the lag time corresponding to the largest absolute value of correlation coefficient. Positive coefficients indicate that the signals are in-phase with one another (i.e., positive correlation), and negative coefficients indicate the signals are out-of-phase, where an increase in one signal corresponds to a decrease in the other (i.e., negative correlation). The data shown in figure 3(b) summarize that currents produced by all three bilayers in the asymmetric array are positively correlated with a time lag of 0.18 ms. In other trials (not shown), multiple membranes aligned on the same side of the hair again exhibited positive correlations, indicating that currents are nearly 'in-phase'. The small time lag per successive droplet interface averages between 0.18 and 0.20 ms, which for vibration of the hair 158 Hz, corresponds to a phase angle of ca. 8.1°. Separately, cross-correlation analysis of the two bilayers for the symmetric three-droplet, two-bilayer array showed a negative maximum correlation coefficient at a time lag of 0.13 ms, confirming quantitatively that the currents are $180° \pm 6.1°$ 'out of phase' (figure 3(b)).

This information provides insight into the relative motions of the multiple membranes in each array during hair perturbation. Recall that the current produced by a membrane is a function of both the applied voltage and the dC/dt caused by transverse bending of the bilayer during vibration [55]. Thus, the sign of the sensing current from a given membrane depends on both the sign of the transmembrane potential and whether bending produces a positive or negative time rate of change in capacitance. In these experiments, positive bilayer current is defined as that which flows in the direction of decreasing potential. Because all membranes are biased with a positive potential, negative current instead results from decreases in dC/dt. Because the membranes in an asymmetric array yield currents that are nearly 'in-phase' for voltages of equal sign indicates that they experience deformations that are also nearly 'in-phase'. Because our previous studies [55, 61] have shown that transverse membrane bending is the primary mode of deformation, we interpret a positive dC/dt to correspond to an increase in bilayer

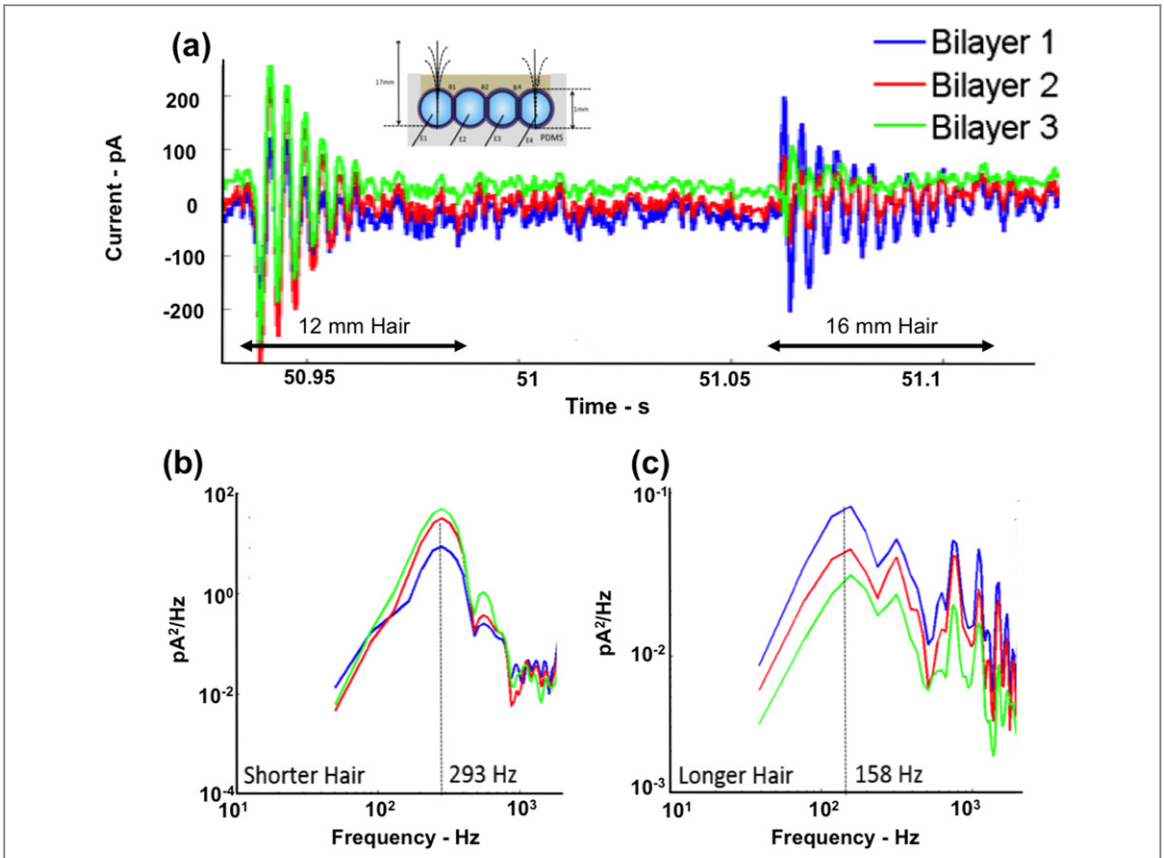

Figure 4. (a) Currents of three bilayers in response to flicks of a short and then long hair. PSDs of the currents produced by flicking the 15–17 mm hair (b) and the 11–13 mm hair (c).

curvature (and thus surface area). A negative dC/dt value in an oscillation cycle, conversely, corresponds to when the membrane flattens. Using this process, we conclude that the 'in-phase' currents produced by the asymmetric array indicate that these interfaces experience increases and decreases in curvature together with minor phase delays due to viscous damping. This same analysis also suggests for the three-droplet symmetric array that one membrane becomes more curved while the other loses curvature. The missing detail in this process is whether interfaces that respond 'in-phase' with one another experience curvature in the same direction, The schematics in the table in figure 3(b) summarize how the phase differences in sensing currents relate to the relative deformations of the bilayers in serial arrays.

3.3. Distinguishing perturbations of separate hairs in a serial array

Because vibrational energy dissipates with distance, a larger array of droplets may need multiple hairs to effectively distribute a perturbation to the network or locally excite specific membranes. Thus, we consider a variation of the original 5-droplet, 4-bilayer array shown in figure 1, which now includes a second, 14 mm hair inserted into a different droplet. Different lengths for the two hairs are intentionally selected to separate their characteristic frequencies of vibration. This system was comprised of four droplets connected in series to form three bilayers, with hairs placed in the end droplets as shown in the inset in figure 4(b). A 5-droplet series was not used since the fourth bilayer in a series was shown to produce minimal response to flicking (figure 2(a)). Per the inset in figure 4(a), the flicker bends and releases (moving right to left) the shorter hair in the fourth droplet and then flicks the longer hair located in the first droplet. Figure 4(a) also shows the currents generated by each lipid membrane in response to the two flicks. As shown by the arrows in this figure, the first set of underdamped current responses is due to perturbation of the shorter hair, while the second series of responses are generated when the flicker strikes and releases the longer hair. The largest current from the first flick comes from bilayer 3, which is positioned nearest to the shorter hair, and the smallest current comes from bilayer 1, which is the farthest bilayer from this hair. In contrast, bilayer 1 produces the largest current and bilayer 3 generates the smallest response when the flicker perturbs the longer hair. In addition to spatial differences, we observe in figure 4(a) that flicking the shorter hair produces larger currents from all three membranes than when the longer hair is perturbed. This difference is explained by the shorter hair's higher

bending stiffness, which allows it to transmit more energy into the adjacent droplets upon flicking.

PSDs of these same sensing currents reveals a predominant peak frequency at 293 Hz in all three currents when the shorter hair is flicked (figure 4(b)) and a separate peak at 158 Hz in all three signals when the longer hair is flicked (figure 4(c)). The higher frequency peaks (>800 Hz) in the spectrogram correspond primarily to harmonics of 60 Hz noise. These results confirm that membrane vibration is driven by hair motion, and they provide proof that all three bilayers in the array are able to respond to motion by either hair. Recall, the fundamental natural frequency, ω_n, of a cantilever beam in bending is proportional to the square root of the product of the elastic modulus, E, and the cross-sectional area moment of inertia, I, and inversely proportional to the square root of the product of mass per unit length, m, and the fourth power of beam length, l, as given by

$$\omega_n \propto \sqrt{\frac{EI}{ml^4}}. \quad (2)$$

Thus, the ratio of natural frequencies for hairs that differ only in length is given by:

$$\frac{\omega_l}{\omega_s} = \frac{l_s^2}{l_l^2}. \quad (3)$$

The subscripts l and s are used to denote the longer and shorter hairs, respectively. Comparing the ratio of measured peak frequencies (158 and 293 Hz) to the ratio of the squares of hair free lengths (17 mm and 12 mm, respectively) as given by equation (3) shows that they have very similar values (0.54 and 0.50, respectively) and confirms that both hairs respond as cantilevered beams in the system. While the oil and water droplets also likely contribute to the measured natural frequencies of the sensing currents, the fact that the frequency content of the bilayer currents are directly related to the natural frequencies of the hairs shows that multi-bilayer arrays can be used to provide frequency selectivity by tuning the natural frequency of the hair. In summary, this experiment shows that the relative magnitudes and characteristic frequencies of bilayer sensing responses can be used to distinguish motions of multiple hairs in an array, which could be used to investigate differences in perturbation timing and direction.

4. Modeling mechanotransduction

In this section, we aim to establish an order of magnitude approximation for the sensing current generated by the lipid membrane in response to prescribed airflow to provide physical insights into how single and multiple membrane networks can be used to sense mechanical perturbations. Describing the complete transduction process requires knowing separately: (1) how airflow affects hair motion; (2) how hair motion induces forces on nearby bilayers; (3) how this force drives membrane deformation; and (4) how dynamic changes in deformation state create variations in capacitance that generate current.

4.1. Airflow induced hair motion

Estimating the motion of a small-diameter hair induced by turbulent airflow is not trivial. The theoretical basis for describing hair motion in our transduction model employs Stoke's theory of pendulum motion in a fluid medium [58] to describe how the surrounding fluid augments the total drag and inertia of the hair in addition to acting as a forcing function that induces motion. Several prior studies on modeling the motion of insect hairs [13, 20, 28] also utilized Stoke's theory; the authors justified the use of a rigid-body model for hair motion based on observations that these insect hairs rotate and do not bend when perturbed. The use of Stoke's theory is not constrained to rigid body motion. Park, *et al* [43] more recently applied Stoke's concepts of airflow induced drag and inertia to a cantilevered hair structure that underwent flow-induced bending in a single fluid medium. Motion was simulated by solving for the forced response of a distributed parameter model of a continuous hair with augmented (but constant across the length of the hair) damping and mass per unit length coefficients.

Our system is more complex in that the hair in a DIB-based sensor extends through multiple liquid media. Since the fluid media provide both driving forces that induce motion as well as adding drag and inertia to the beam, multiple layers of fluid creates an inhomogeneous cantilevered beam, whose effective damping and mass per unit length are different in each fluid layer. Therefore, to avoid the need for finite element methods [9] to approximate the bending response of an inhomogeneous hair and to retain an analytical model for describing how airflow creates hair motion, we choose to approximate the hair's motion as pure rigid body rotation (i.e. no bending).

The dynamic hair system considered herein is shown in figure 5(a). This schematic shows a rigid, cylindrical hair with density, ρ_{hair}, radius, r_h, and total free length, l, that is supported by a solid substrate at the lower end and which extends in the y-direction through a shallow liquid layer of height, b, that represents the water droplets and oil. Horizontal airflow is applied across the top portion of the hair from a height $y = d$ to the free end at $y = l$. The hair has a mass moment of inertia, I_h, with respect to the axis of rotation at the fixed end where a torsional spring with spring constant, k_t, is included to represent the restoring torque provided by the substrate. Note the value of k_t is fitted manually in this model to achieve a similar lateral tip motion of the hair as measured during experiments. In the absence of the fluid layers and

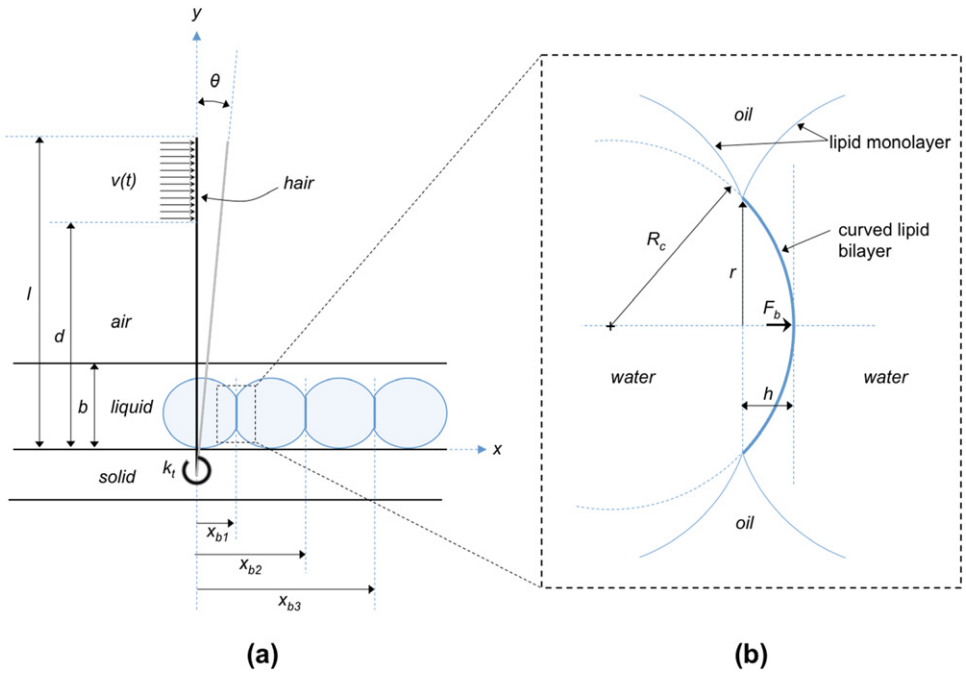

Figure 5. (a) Side view of a membrane-based hair cell sensor shows that the hair extends through two fluid media. (b) Side view of the geometry of a single lipid bilayer bending in response to an applied point force.

applied airflow, the equation of motion in terms of the rotational angle, θ, is

$$I_h\ddot{\theta}(t) + k_t\theta(t) = 0. \quad (4)$$

To perturb the hair, we assume a uniform, horizontal airflow extending from the surface of the liquid to the top of the hair with sinusoidal velocity in time given by

$$v(t) = v_o\sin(\omega t), \quad (5)$$

where v_0 is the amplitude and $\omega = 2\pi f$ is the angular frequency. While our own experiments have utilized steady airflow to perturb the hair, we observe the hair to undergo oscillatory motion as it bounces in and out of the air stream. Further, the transduction mechanism for current generation depends on a time rate change in capacitance, as opposed to a static change that could be caused by static bending of the hair. Thus, we assume that an oscillatory airflow, which can be thought of as a time changing torque on the hair's motion, $T_{\text{air}}(t)$, provides a good approximation of the driving force for hair motion.

The liquid layer near the supported lower end is assumed to be still. Nonetheless, modeling this layer of fluid using the same approach as that for the air medium [58] is necessary to approximate the drag and momentum that it adds to the hair. Similarly, the net effect of this layer is also that of a time dependent torque, $T_{\text{liq}}(t)$, such that

$$I_h\ddot{\theta}(t) + k_t\theta(t) = T_{\text{air}}(t) + T_{\text{liq}}(t). \quad (6)$$

To find explicit expressions for $T_{\text{air}}(t)$ and $T_{\text{liq}}(t)$ in terms of θ and v, we consider that both fluid layers exhibit moments on the hair that depend on the horizontal relative velocity, $v - y\dot{\theta}$, and acceleration, $\dot{v} - y\ddot{\theta}$, of the fluid with respect to the hair. Using Stokes' theory to model the drag-induced and moment-induced forces per unit length caused by these fluid layers on the hair and integrating them over the portion of the hair's length in each fluid (see section 3 in SI for details), we obtain expressions (equations (S12) and (S13)) for the total torque generated by airflow in terms of the airspeed and its derivative and the derivatives of the rotational coordinate, θ. This result indicates that the air layer (including the still portion from $0 \leqslant y < d$ and the flow field from $d \leqslant y \leqslant l$) acts as both a forcing function dependent on airspeed (1st group in equation (S22)) as well an added source of viscous damping and inertia dependent on hair rotation (2nd group in equation (S22)). A similar approach is pursued to obtain expressions (equations (S18) and (S20)) for the drag and inertia-based torques on the hair from the still liquid layer. However, because the liquid layer has zero velocity, the total moment induced by this fluid (equation (S23)) is only a function of the coordinate of rotation, θ, implying that the liquid layer does not drive motion, but only adds viscous damping and inertia to the equation of motion for the hair.

Combining the drag and inertia-induced moments in air and under liquid allows the complete equation of motion for the hair to be rewritten as

$$(I_h + I_{\text{air}} + I_{\text{liq}})\ddot{\theta}(t) + (c_{\text{air}} + c_{\text{liq}})\dot{\theta}(t) + k_t\theta(t) = \left(\frac{l^2 - d^2}{2}\right)(A_1\nu(t) + A_2\dot{\nu}(t)), \tag{7}$$

where

$$\begin{aligned} I_{\text{air}} &= A_2\left(\frac{l^3 - b^3}{3}\right), \\ I_{\text{liq}} &= A_4\left(\frac{b^3}{3}\right), \\ c_{\text{air}} &= A_1\left(\frac{l^3 - b^3}{3}\right), \\ c_{\text{liq}} &= A_3\left(\frac{b^3}{3}\right). \end{aligned} \tag{8}$$

Expressions for the terms A_1–A_4 are described in the SI. Solving equation (7) can be used to compute the resulting motion of the hair in response to varying airflow speeds and liquid layer heights. Inspection of equation (7) confirms that when the liquid layer is removed (i.e. $b = 0$, and the full length of the hair resides in air), the added inertia and damping only come from the airflow. Second, the equation of motion also confirms that when the hair is fully submerged in still liquid ($b = l$), the forcing term on the right hand side is zero, which means the hair remains unperturbed by airflow above the liquid layer. The steady-state amplitude of hair rotation is given by

$$|\theta| = \left[\frac{\sqrt{(M_1)^2 + (M_2\omega)^2}}{\sqrt{(k_t - \omega^2 I_t)^2 + (c_t\omega)^2}}\right]\nu_0, \tag{9}$$

where

$$\begin{aligned} M_1 &= A_1\frac{l^2 - d^2}{2}, \\ M_2 &= A_2\frac{l^2 - d^2}{2}, \\ I_t &= I_h + I_{\text{air}} + I_{\text{liq}}, \\ c_t &= c_{\text{air}} + c_{\text{liq}}. \end{aligned} \tag{10}$$

Finally, the undamped natural frequency, ω_0 (rad s^{-1}), of the coupled fluid-structure system is given by the square root of k_t/I_t.

4.2. Transmitted force on bilayer generated by hair motion

The first part of the model yielded a relationship (equation (9)) between the speed of an applied sinusoidal airflow and the resulting rotational vibration of the hair. Now, we focus on the link between hair vibration and the force transmitted to a nearby lipid bilayer. Just as the liquid layer induces a net moment on the hair because of its motion, the hair contributes a resulting moment (and force) of the same magnitude on the fluid. While this moment is distributed from 0 to b, an effective point force under steady-state hair motion exerted at y_b, the height at which the center of the bilayer is positioned, can be written as

$$F_{\text{hair}} = \frac{|T_{\text{liq}}|}{y_b}. \tag{11}$$

The magnitude of total liquid-induced moment at steady-state is given by

$$|T_{\text{liq}}| = \frac{b^3}{3}(\sqrt{(A_3\omega)^2 + (A_4\omega^2)^2})|\theta|, \tag{12}$$

where the rms is used since the drag-induced torque (which depends on rotational velocity) and inertia-induced torque (which depends on the rotational acceleration) do not occur in phase. Equation (11) estimates the total resultant force the hair exerts on the liquid layer. Stokes previously demonstrated that a solid plane moving through a fluid creates a propagating normal pressure front that decays as it moves away from the solid–liquid interface [58]. Specifically, at a distance x away from the plate, Stokes predicted that the normal pressure, $P(x)$, to be given by

$$P(x) = 4\mu_{\text{fluid}}\nu_0\sqrt{\frac{2\pi f}{\nu_{\text{fluid}}}}e^{-\sqrt{\frac{2\pi f}{\nu_{\text{fluid}}}}x}, \tag{13}$$

where μ_{fluid} and ν_{fluid} are the dynamic (shear) and kinematic viscosities of the fluid, respectively, and v_0 and f are the speed and frequency of oscillating airflow. This means that at a distance $x = x_{\text{bi}}$ away from the hair, the magnitude of the force acting on the ith membrane is exponentially less than it is at the surface of the hair. Furthermore, since our system considers a small-diameter cylindrical hair rather than an infinite flat plate moving in a fluid, we expect there to be an even lower efficiency in transmitting force through liquid from the hair to the bilayer. Because of both factors, we choose instead to describe the net force acting on both the adjacent and successive membranes present in a droplet array as empirical fractions of that exerted by the hair on the fluid:

$$F_{\text{bi}} = \beta_i F_{\text{hair}}, \tag{14}$$

where the efficiency of transmitted force, $\beta_i \ll 1$ and $\beta_i > \beta_{i+1}$. Combing equations (9), (10), and (13) allows the magnitude of the force on the ith bilayer, F_{bi}, to be directly related to the magnitude of hair rotation:

$$F_{\text{bi}} = \beta_i\left[\frac{b_3}{3y_b}(\sqrt{(A_3\omega)^2 + (A_4\omega^2)^2})|\theta|\right]. \tag{15}$$

This approach allows the value of β to be estimated empirically from measurements of bilayer currents induced by airflow at a known flow rate and frequency of vibration.

4.3. Deformation response of a lipid bilayer to an applied force

The following derivation considers the deformation of a circular, planar bilayer with a radius, r, and a fixed hydrophobic thickness, t, where $t \ll r$. The circular membrane is assumed to be pinned along its circumference such that the application of a centered,

transverse force results in a rotationally symmetric deflection of constant curvature (figure 5(b)). It is well established that it is much easier to bend a lipid bilayer than it is to laterally stretch it [8, 34]. Further, if the membrane is assumed to be intrinsically flat, which is the case for DIBs formed between identical droplets [14], then Helfrich showed [5, 8, 23] that the free energy per unit area stored in bending is

$$f_B = \frac{1}{2}\kappa J^2 + \bar{\kappa}K, \tag{16}$$

where, κ and $\bar{\kappa}$ are the bending and Gaussian moduli of elasticity for the membrane, J is the total membrane curvature and K is the Gaussian curvature. For a circular membrane under radially-symmetric bending in the shape of a spherical cap, J is the sum of equal principle curvatures, each with radius, R_c, and K is the product of the two principle curvatures. Using these definitions, we can rewrite the energy per unit area of bending in terms of the radius of curvature for the membrane

$$f_B = \frac{2\kappa + \bar{\kappa}}{R_c^2}. \tag{17}$$

The total energy due to bending is then found by multiplying f_B by the area of the deformed membrane, A_b, where $A_b = 2\pi R_c h$ and h is the height of the spherical cap at the center of the bilayer (figure 5(b)). This substitution shows that the total energy of bending, E_B, is determined by the geometrical parameters (R_c and h) and the elastic moduli (κ and $\bar{\kappa}$), as given by

$$E_B = \frac{2\pi h(2\kappa + \bar{\kappa})}{R_c}. \tag{18}$$

Equation (18) represents the total amount of stored energy in a membrane deformed from a flat state into a spherical cap with radius, R_c, and height, h. To relate this to the motion of the hair, we relate the stored energy to the work done on the membrane by an equivalent point force on bilayer, F_b, positioned at the center bilayer. Assuming this force, which induces transverse deflection at the center (figure 5(b)), varies linearly with distance at small deflections, the work done to create a spherical cap of height, h, is

$$W_F = \frac{1}{2}F_b h. \tag{19}$$

Ignoring damping in the membrane's response, we can thus treat the dynamic displacements observed experimentally as discrete, quasi-static solutions, where the work done by the horizontal force, W_F, is equal in magnitude to the energy of bending, E_B, in the bilayer, as written by

$$R_c = \frac{4\pi(2\kappa + \bar{\kappa})}{F_b}. \tag{20}$$

This relationship results in an expression that inversely relates the applied force, F_b, to the induced radius of curvature, R_c, of the bent membrane. Note that h cancels, leaving R_c as a solvable term for known values of bending moduli and input force. Equation (20) thus provides a way to compute the amount of deformation created by an applied force in the transverse direction, and it can easily be rewritten in terms of an equivalent mechanical pressure acting on the bilayer by multiply by the projected area, A, of the bilayer.

4.4. Electrical response to mechanical deformation

It has been shown [55, 61] that the magnitude of capacitive sensing current, i, generated by the membrane hair cell is given by equation (1), where, dC/dt represents the time rate of change in membrane capacitance caused by mechanical deformation of the bilayer, V is the transmembrane voltage, and α is the electrowetting constant. To arrive at a mechanoelectrical model for the membrane, we must relate dC/dt to the state of deformation in the membrane and its intrinsic capacitance per unit area, C_m. Modeled as a parallel plate capacitor, the capacitance per unit area of a bilayer describes the ratio of dielectric permittivity, ε, to the thickness, t, for the hydrophobic region of the membrane [63], as given by

$$C_m = \frac{C}{A} = \frac{\varepsilon}{t}. \tag{21}$$

Values of C_m for synthetic lipid bilayers range from 0.1 to 1.0 μF cm^{-2}, depending on the length and type of the lipid acyl chains and the amount of trapped oil in the membrane [63]. DPhPC bilayers formed in hexadecane as used herein exhibit a membrane capacitance of 0.65 μF cm^{-2} [63]. Assuming that when the membrane is deformed, neither its thickness or permittivity change, then C_m is constant. This means that the total change in bilayer capacitance must instead result from the change in area incurred by bending, as written by

$$\Delta C = C_m \Delta A = C_m(2\pi R_c h - \pi r^2), \tag{22}$$

where r is the radius of the flat, circular membrane. For $h > 0$, $R_c > r$, and $h > R_c$ the height of the spherical cap, h, can be written as:

$$h = R_c - \sqrt{R_c^2 - r^2}. \tag{23}$$

This relationship enables equations (22) and (20) to be combined to express the change in capacitance, ΔC, as a function of a transverse equivalent force, F_b.

The time required for the membrane to exhibit this change in capacitance depends on the initial deformation state of the membrane. For a perfectly flat membrane, where symmetric deformation to a bent state causes an increase in capacitance for bending in both directions, the capacitive current occurs at twice the frequency of the applied force [41]. Ochs and Petrov referred to this as the microphone effect [41, 46]. However, if the bilayer is initially curved, then an oscillating force increases the capacitance as curvature increases and then decreases capacitance as the membrane returns toward a flatter state. Because these

increases and decreases occur in phase with the magnitude of the force, the induced current occurs at the same frequency as the source of mechanical excitation [41]. Therefore the bilayer can exhibit changes in capacitance at one and two times the frequency of the input.

In our prior study, power spectral analysis of the frequency of measured capacitive currents in single-membrane hair cells demonstrated that energy in the current signal is evenly distributed at both the same frequency as the hair's motion as well as at two times this frequency [61]. This finding suggests that the membrane likely transitions between vibrating from a flat equilibrium condition to one that is distended to one side [41]. Previously, we approximated this multi-mode response with a double sinusoidal capacitance waveform, given by

$$C(t) = C_1 \sin(\omega t) + C_2 \sin(2\omega t), \tag{24}$$

where C_1 and C_2 are the amplitudes of capacitance variation at one and two times the driving frequency, ω, respectively, to derive a relationship between the magnitude of the total change in capacitance, $|C|$, as a function of the measured rms dC/dt:

$$|C| \approx 1.3 \frac{1}{\sqrt{2}\,\omega} \left(\frac{dC}{dt}\right)_{\text{rms}}. \tag{25}$$

Here we can instead use equation (25) to compute the rms value of dC/dt for a known amplitude of change in capacitance, assumed to be equal to that given by equation (11) ($|C| = \Delta C$), as shown by

$$\left(\frac{dC}{dt}\right)_{\text{rms}} \approx \frac{\sqrt{2}\,\omega}{1.3} \Delta C. \tag{26}$$

Substituting equation (22) into equation (26), and then this result into equation (1) provides an expression for the rms value of capacitive current induced by dynamically deforming the membrane at a frequency of ω

$$(i)_{\text{rms}} = \left[\frac{\sqrt{2}\,\omega}{1.3} C_m (2\pi R_c h - \pi r^2)\right](V + \alpha V^3). \tag{27}$$

If instead, the membrane were assumed to produce current only at twice the frequency of the input stimulus (i.e. the microphone effect), then the time rate of change in capacitance can be computed from the change in capacitance that occurs in the first ¼ of an oscillation period, T, at which the capacitance reaches a maximum. Recalling that in this situation T is equal to the reciprocal of twice the frequency, the time rate of change in capacitance can be written as

$$\left(\frac{dC}{dt}\right)_{\text{rms}} \approx \frac{2\sqrt{2}\,\omega}{\pi} \Delta C. \tag{28}$$

Now, combining equations (1), (22), and (28), we obtain an expression for the magnitude of rms current produced by a capacitive lipid bilayer that oscillates at twice the driving frequency, ω:

$$(i)_{\text{rms}} = \left[\frac{2\sqrt{2}\,\omega}{\pi} C_m (2\pi R_c h - \pi r^2)\right](V + \alpha V^3). \tag{29}$$

4.5. Comparison of simulated and measured hair cell responses

Figure 6 compares the predicted and measured steady-state tip motions of a hair versus airspeed when a horizontal stream of airflow is distributed across the top 15% of the free length of the hair. The model treats the velocity of the applied airflow as a sinusoidal waveform; a driving frequency of 160 Hz is selected to mimic the observed oscillatory hair motion near this same frequency when a narrow stream of airflow is applied to the hair. The simulations consider a hair with a radius, free length, and density of 45 μm, 17 mm, and 1100 kg m^{-3}, respectively. The model also considers that ~24% of the free length of the hair is submerged under liquid (i.e. $b = 4$ mm), which is modeled as a single homogeneous medium with a viscosity of 1.5×10^{-5} m^2 s^{-1} and density of 900 kg m^{-3}. These values represent the averages of viscosity and density for aqueous droplet and oil present at the base of the hair in the experiments. Finally, the predicted hair motion is calculated for five different values of undamped natural frequency to illustrate the effect of this variable on simulated hair motion.

Figure 6(a) shows the steady-state lateral tip motion predicted for a rigid hair that undergoes pure rotation in response to the sinusoidal flow. The lateral motion is computed as the product of the free length of the hair and the sine of the steady-state hair's rotation angle, θ, as given in equation (9) (see figure S3 in the SI for a complementary plot of the computed steady-state amplitude of the rotation angle versus airspeed). These calculations show that the maximum amount of hair rotation is ca. 10°, which occurs at the highest velocity of 20 m s^{-1}. The measured data points and error bars represent the mean displacement of the hair ±1 standard deviation, respectively, determined with an anemometer during $n = 3$ separate 10 s trials at each airspeed on a single 17 mm long hair supported as shown in figure 1. Both the measured and predicted displacements show that tip displacement varies linearly with respect to air velocity. The simulated tip motions in figure 6(a) show that a value of ca. 155–165 Hz for $f_0 = \omega_0/(2\pi)$ yields predicted tip displacements that fit well to the measured amplitudes of tip motion versus airspeed. Since the airflow is assumed to oscillate at 160 Hz, this match in tip displacements indicates that the hair operates near resonance (likely as a result of the hair bouncing in and out of the narrow flow, or due to vortex-induced vibrations). Since hair vibration at resonance is expected to occur at a frequency that is lower than f_0, we utilize an assumed value for f_0 of 162 Hz for the remainder of the

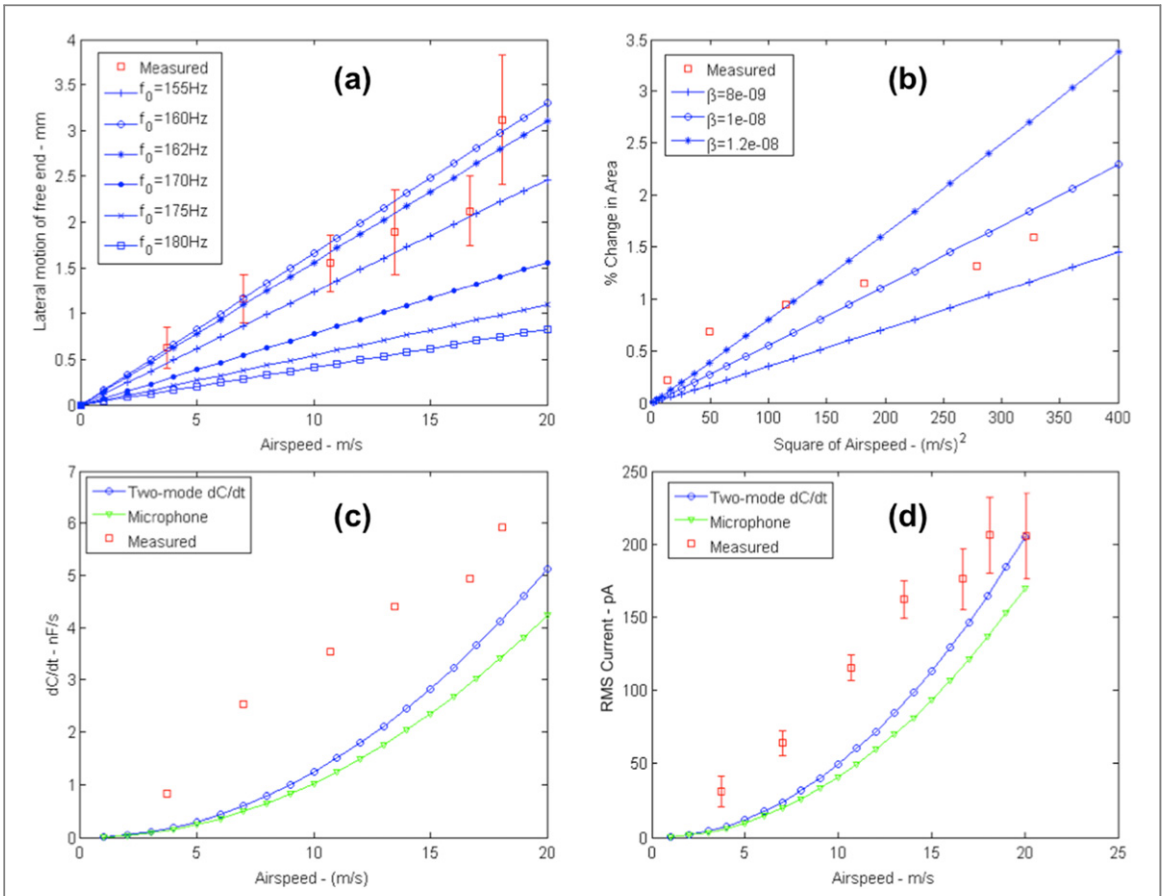

Figure 6. Comparisons between model predictions and data obtained on a two-droplet membrane based hair cell: (a) lateral motion of the tip of the hair versus airspeed; (b) percent change in bilayer area versus airspeed; (c) time rate of change in bilayer capacitance, dC/dt, versus airspeed, and (d) rms current versus airspeed for an applied voltage of 40 mV. Predictions for two-mode vibration (equation (27)) and single-frequency microphone effect (equation (29)) are provided in (c) and (d).

calculations regarding the membrane's response to this oscillation.

In addition, transient hair motion (shown in figure S4 in the SI by solving equation (7) in response to a still initial condition for the hair) predicted by the model exhibits a time to reach steady state of approximately 0.12 s, which compares closely to the decay times observed for the flicking responses shown in figures 1(a), 2(a), and 3(c). These results provide good evidence that the tip motion of a rigid hair in response to a sinusoidal airflow matches suitably to that observed for steady airflow across a flexible hair used in experiments.

These data were also used to predict the equivalent point force induced by the hair on the fluid at a height, y_b, equal to the center of the droplets (located 0.5 mm up from the pinned end) as given by equations (11) and (12). Because the motion of the hair varies linearly with airspeed, we find this force also varies linearly versus airspeed with a sensitivity of 63 nN m^{-1} s^{-1} (see figure S5a in the SI). Therefore, at a speed of 20 m s^{-1}, the model for a rigid hair oscillating at 160 Hz in both liquid and air predicts that the hair creates a force in the direction of its own motion with a magnitude of ca. 1.26 μN.

Figure 6(b) compares measured values of percent change in bilayer area versus applied airspeed to those predicted from the radius of curvature of the deformed bilayer (equation (20)) using the expression for change in area shown in equation (22). Calculating bilayer deformation requires selecting a value for the force transmission efficiency, β, that dictates the effective point force applied to the center of the membrane; here, three values of β are used to demonstrate the relative magnitude and sensitivity of this selection on the predicted force and resulting membrane deformation. This parameterized calculation shows that a β value of ca. 1×10^{-8} provides a reasonable match between membrane deformation versus airspeed. Note that a 3% dynamic change in membrane area at 20 m s^{-1} is reasonable, and consistent with prior studies which showed membrane rupture occurs under static loading at stretch ratios of 2%–5% [39].

Such a small value for β signifies that the amount of force transferred from the motion of the hair to the membrane is on the order of fN (see figure S5b in the SI). This is not surprising since the liquid environment surrounding the hair is expected to result in poor force transmission to the membrane some distance away from the hair. However, the small β may also suggest that the model overestimates the force incurred on the

fluid because of an overestimate in the hair motion itself (equation (11)) that would result from a hair undergoing bending in addition to rotation. Pure bending of a cantilevered hair would dictate very small amounts of transverse deflection near the fixed end; thus our estimate of hair motion at a height corresponding to the center of the bilayer may be artificially high. Nonetheless, both the data and predicted values show a similar, approximately linear relationship between the amplitude of bilayer area change versus flow speed.

The remainder of the simulated membrane response versus applied airspeed shows that model captures well the electrical measured changes in a circular membrane that has a radius of 100 μm and a specific capacitance of 0.65 μF cm^{-2} (figures 6(c) and (d)). The measured data in figure 6(c) represent single estimates of dC/dt computed from the slopes of rms current versus voltage collected at multiple airspeeds on a single membrane, hence no error bars are provided. However, the measured data and error bars in figure 6(d) represent the average values ± 1 standard deviation for dC/dt and sensing current measured at each flow speed for $n = 3$ separate single-membrane sensors that featured the same hair (i.e. each trial used the same substrate and hair but with new droplets and a new bilayer). In comparisons of both dC/dt and rms current, the simulated responses show that a two-frequency capacitive current generates a higher response that a single mode response at the same frequency of the hair's motion. The fact that both predictions underestimate the total dC/dt and rms current may indicate current developed by the membrane does not occur just at these two frequencies but also includes motion across a range of frequencies. It is also possible that the thickness and specific capacitance of the membrane vary slightly during vibration, which would cause our use of values measured in a static configuration to undervalue the change in capacitance at a given voltage.

5. Discussion

While several prior works have considered multi-membrane networks for collective transport and mechanotransduction, this study marks the first complete mechanotransduction study of serially linked DIBs, which feature more than 1 lipid bilayer that are physically coupled to other membranes through adjoining droplets. First, we showed experimentally that the capacitive mechanotransduction currents generated by either flicking or airflow across a vertical hair that cause it to vibrate depend on the placement and properties (e.g. length) of the hair in the droplet array. Intuitively, membranes positioned closest to the hair undergo the highest motions and generate the largest currents, while those positioned successively farther away generate smaller responses. Using ~1 mm aqueous droplets, we found that the sensing current typically falls below the detection limit by the 4th membrane away from the hair. Since membranes positioned on the same side of the excited hair produce sensing currents that are generally 'in-phase,' it is also possible to constructively add the sensing currents of each bilayer (figure S1 in SI). This result highlights the potential for greater signal per unit volume with a multi-interface droplet array.

In our prior study on a single membrane hair cell [61], we found that the directionality of the hair motion relative to the membrane and the mechanical stiffness of the aqueous compartments are also important factors on the sensing response. Thus, we would also expect membranes positioned orthogonally to the motion of the hair in a DIB array to undergo the highest transverse displacements and produce the largest currents. Comparing the responses of membranes positioned at different angles with respect to hair motion could be used to decode the direction of an applied mechanical stimulus. Likewise, creating arrays from aqueous compartments using hydrogels [50, 56] could used to stiffen the volumes, thereby increasing force transmission to each bilayer and causing larger bilayer deformations and currents [61]. This effect may also allow for membranes positioned farther from the hair to transduce its motion.

The transduction model presented demonstrates that the physical properties of the hair and the dynamics of the hair's motion, as well as the area, thickness, dielectric permittivity, and bending modulus of the interfacial membrane dictate the amount of membrane deformation and change in capacitance that produces current. In this work, the model was implemented to predict the sensing current generated by a single membrane adjacent to a hair perturbed by airflow. Figure 6 shows that we achieved a suitable approximation for the tip motion of a hair perturbed by airflow, as well as the change in capacitance and current by the membrane when a transmission efficiency factor, β, was selected to adjust the force applied to the membrane. These predictions can be extended to additional membranes in an array by utilizing empirically derived decay rates such as those found from the data of successive bilayer currents shown in figure 2. The primary limitations of our model include the facts that: (1) a rigid body model for hair motion likely overestimates the displacement of the hair at a height near the bilayer; and (2) we cannot exactly predict or measure both the force applied to the membrane and the dynamic shape of the bilayer as it vibrates.

Nonetheless, our findings demonstrate for the first time the value of using an array of multiple lipid bilayers formed with more than two droplets to increase the magnitude of total sensing response and to enable distributed membrane-based sensing of hair motion for more than one hair in an array. This advance showcases the evolution of this system from a single hair, single membrane sensor to a higher-order functional assembly comprised of many droplets arranged 2D. Further, when combined with methods to encapsulate

liquid-supported DIBs in a sealed-solid material using either a microfluidic approach [40] or via direct encapsulation of DIBs in a solid-organic phase (*manuscript in preparation*), we believe multi-membrane DIBs can enable the development of membrane-based bio-inspired materials that can perform mechanotransduction—i.e. feel their surroundings by sensing physical stimuli that cause the encased membranes to deform—in ways similar to how animals sense mechanical disturbances. To enable hair cell functionality in a fully-sealed assembly, we would need to add a hair structure that passes from the enclosed droplets through the sealing layer such that it could interact with a surrounding medium, such as water, which would normally displace (due to density differences or hydrodynamic flows) the oil and water droplets or contaminate the system in a way that prevents reliable lipid self-assembly.

In summary, we view potential applications of membrane-based materials, such as DIB-based hair cells as well as intra-droplet membranes formed from amphiphilic surfactants [2] or polymers [62] synthesized specifically to tune membrane properties, as being similar to those performed by the hair cells of living creatures, e.g. vibration sensing, flow detection, tactile sensing, and acoustic response. The reliability of this device demands that the membrane not only be durable, but that the interaction between the hair and the membrane(s) be relatively consistent during operation. The use of block copolymer molecules for enhancing membrane stability [67] is one specific method in which the reliability of the membranes could be improved. However, unlike solid-state hair cell inspired sensors built from silicon or polymers, a soft biomolecular approach at sensing offers advantages such as lower cost, the potential for rapid re-assembly to refresh the system, and operation at low-frequency. Additionally, we emphasize that the use of biomembranes for enabling sensing provides a versatile environment for adding additional functionality to the system through the incorporation of transmembrane or membrane-active biomolecules. One example is the use of mechanosensitive transmembrane molecules, which would enable sensing currents in response to membrane stretch [37, 38]. Like in animals, where many hair cells are used to provide multi-modal forms of mechanotransduction, we thus believe the DIB can enable new forms of membrane-based sensing arrays that exhibit spatially, directional, and frequency selectivity to a variety of physical inputs including vibration, fluid flow, and also acoustic pressure.

Acknowledgements

The authors gratefully acknowledge financial support from Air Force Office of Scientific Research, Basic Research Initiative Grant Number FA9550-12-1-0464.

References

[1] Ashmore J 2008 Cochlear outer hair cell motility *Physiol. Rev.* **88** 173–210
[2] Astafyeva K, Urbach W, Garroum N, Taulier N and Thiam A R 2015 Stability of C12Ej bilayers probed with adhesive droplets *Langmuir* **31** 6791–6
[3] Baconguis I and Gouaux E 2012 Structural plasticity and dynamic selectivity of acid-sensing ion channel-spider toxin complexes *Nature* **489** 400–5
[4] Barth F G 2002 Spider senses—technical perfection and biology *Zoology* **105** 271–85
[5] Bassereau P, Sorre B and Lévy A 2014 Bending lipid membranes: experiments after W Helfrich's model *Adv. Colloid Interface Sci.* **208** 47–57
[6] Bayley H, Cronin B, Heron A, Holden M A, Hwang W L, Syeda R, Thompson J and Wallace M 2008 Droplet interface bilayers *Mol. BioSyst.* **4** 1191–208
[7] Bruhn B R, Schroeder T B, Li S, Billeh Y N, Wang K and Mayer M 2014 Osmosis-based pressure generation: dynamics and application *PloS One* **9** e91350
[8] Campelo F, Arnarez C, Marrink S J and Kozlov M M 2014 Helfrich model of membrane bending: from Gibbs theory of liquid interfaces to membranes as thick anisotropic elastic layers *Adv. Colloid Interface Sci.* **208** 25–33
[9] Chakraborty A, Gopalakrishnan S and Reddy J 2003 A new beam finite element for the analysis of functionally graded materials *Int. J. Mech. Sci.* **45** 519–39
[10] Creasy M A, Freeman E C, Philen M K and Leo D J 2015 Deterministic model of biomolecular networks with stimuli-responsive properties *J. Intell. Mater. Syst. Struct.* **26** 921–30
[11] Crissman H, Mullaney P and Steinkamp J 1975 Methods and applications of flow systems for analysis and sorting of mammalian cells *Methods Cell Biol.* **9** 179–246
[12] Dallos P and Evans B N 1995 High-frequency motility of outer hair cells and the cochlear amplifier *Science* **267** 2006–9
[13] Devarakonda R, Barth F G and Humphrey J A C 1996 Dynamics of arthropod filiform hairs: IV. Hair motion in air and water *Phil. Trans. R. Soc. London* **351** 933–46
[14] Dixit S S, Pincus A, Guo B and Faris G W 2012 Droplet shape analysis and permeability studies in droplet lipid bilayers *Langmuir* **28** 7442–51
[15] Droogendijk H, de Boer M, Sanders R and Krijnen G 2014 A biomimetic accelerometer inspired by the cricket's clavate hair *J. R. Soc. Interface* **11** 20140438
[16] Elani Y, deMello A J, Niu X and Ces O 2012 Novel technologies for the formation of 2D and 3D droplet interface bilayer networks *Lab Chip* **12** 3514–20
[17] Elliott S J and Shera C A 2012 The cochlea as a smart structure *Smart Mater. Struct.* **21** 064001
[18] Engel J M, Chen J, Liu C and Bullen D 2006 Polyurethane rubber all-polymer artificial hair cell sensor *J. Microelectromech. Syst.* **15** 729–36
[19] Fan Z, Chen J, Zou J, Bullen D, Liu C and Delcomyn F 2002 Design and fabrication of artificial lateral line flow sensors *J. Micromech. Microeng.* **12** 655
[20] Fletcher N H 1978 Acoustical response of hair receptors in insects *J. Comput. Physiol.* **127** 185–9
[21] Creasy M A *et al* 2014 Deterministic model of biomolecular networks with stimuli-responsive properties *J. Intelligent Materi. Syst. Struct.* 1045389X14536004
[22] Gross L C, Heron A J, Baca S C and Wallace M I 2011 Determining membrane capacitance by dynamic control of droplet interface bilayer area *Langmuir* **27** 14335–42
[23] Helfrich W 1973 Elastic properties of lipid bilayers: theory and possible experiments *Z. Natforsch.* C **28** 693–703
[24] Holden M A, Needham D and Bayley H 2007 Functional bionetworks from nanoliter water droplets *J. Am. Chem. Soc.* **129** 8650–5
[25] Hudspeth A 1982 Extracellular current flow and the site of transduction by vertebrate hair cells *J. Neurosci.* **2** 1–10
[26] Hudspeth A 1985 The cellular basis of hearing: the biophysics of hair cells *Science* **230** 745–52

[27] Hudspeth A, Choe Y, Mehta A and Martin P 2000 Putting ion channels to work: mechanoelectrical transduction, adaptation, and amplification by hair cells *Proc. Natl Acad. Sci.* **97** 11765–72
[28] Humphrey J A C, Devarakonda R, Iglesias I and Barth F G 1993 Dynamics of arthropod filiform hairs: I. Mathematical modelling of the hair and air motions *Phil. Trans. R. Soc. London* B **340** 423–44
[29] Hwang W L, Holden M A, White S and Bayley H 2007 Electrical behavior of droplet interface bilayer networks: experimental analysis and modeling *J. Am. Chem. Soc.* **129** 11854–64
[30] Kottapalli A G, Asadnia M, Miao J, Barbastathis G and Triantafyllou M S 2012 A flexible liquid crystal polymer MEMS pressure sensor array for fish-like underwater sensing *Smart Mater. Struct.* **21** 115030
[31] Kottapalli A G P, Bora M, Asadnia M, Miao J, Venkatraman S S and Triantafyllou M 2016 Nanofibril scaffold assisted MEMS artificial hydrogel neuromasts for enhanced sensitivity flow sensing *Sci. Rep.* **6** 19336
[32] Liu C 2007 Micromachined biomimetic artificial haircell sensors *Bioinsp. Biomim.* **2** S162
[33] Maglia G, Heron A J, Hwang W L, Holden M A, Mikhailova E, Li Q, Cheley S and Bayley H 2009 Droplet networks with incorporated protein diodes show collective properties *Nat. Nanotechnol.* **4** 437–40
[34] Marsh D 2006 Elastic curvature constants of lipid monolayers and bilayers *Chem. Phys. Lipids* **144** 146–59
[35] McConney M E, Chen N, Lu D, Hu H A, Coombs S, Liu C and Tsukruk V V 2009 Biologically inspired design of hydrogel-capped hair sensors for enhanced underwater flow detection *Soft Matter* **5** 292–5
[36] McGary P D, Tan L, Zou J, Stadler B J, Downey P R and Flatau A B 2006 Magnetic nanowires for acoustic sensors *J. Appl. Phys.* **99** 08B310
[37] Najem J S, Dunlap M D, Rowe I D, Freeman E C, Grant J W, Sukharev S and Leo D J 2015 Activation of bacterial channel MscL in mechanically stimulated droplet interface bilayers *Sci. Rep.* **5** 13726
[38] Najem J S, Dunlap M D, Yasmann A, Freeman E C, Grant J W, Sukharev S and Leo D J 2015 Multifunctional, micropipette-based method for incorporation and stimulation of bacterial mechanosensitive ion channels in droplet *Interface Bilayers* **e53362**
[39] Needham D and Nunn R S 1990 Elastic deformation and failure of lipid bilayer membranes containing cholesterol *Biophys. J.* **58** 997
[40] Nguyen M, Srijanto B, Retterer S, Collier C P and Sarles S A 2016 Hydrodynamic trapping for rapid assembly and in situ electrical characterization of droplet interface bilayer arrays *Lab Chip* submitted
[41] Ochs A L and Burton R M 1974 Electrical response to vibration of a lipid bilayer membrane *Biophys. J.* **14** 473
[42] Pang C, Koo J H, Nguyen A, Caves J M, Kim M G, Chortos A, Kim K, Wang P J, Tok J B H and Bao Z 2015 Highly skin-conformal microhairy sensor for pulse signal amplification *Adv. Mater.* **27** 634–40
[43] Park B K and Lee J S 2012 Dynamic behavior of flexible sensory hair in an oscillating flow *J. Mech. Sci. Technol.* **26** 1275–82
[44] Peleshanko S, Julian M D, Ornatska M, McConney M E, LeMieux M C, Chen N, Tucker C, Yang Y, Liu C and Humphrey J A 2007 Hydrogel-encapsulated microfabricated haircells mimicking fish cupula neuromast *Adv. Mater.* **19** 2903–9
[45] Pelrine R, Kornbluh R D, Pei Q, Stanford S, Oh S, Eckerle J, Full R J, Rosenthal M A and Meijer K 2002 Dielectric elastomer artificial muscle actuators: toward biomimetic motion *SPIE's 9th Annual Int. Symp. on Smart Structures and Materials: Int. Society for Optics and Photonics* pp 126–37
[46] Petrov A G and Usherwood P N 1994 Mechanosensitivity of cell membranes *Eur. Biophys. J.* **23** 1–19
[47] Punnamaraju S and Steckl A J 2010 Voltage control of droplet interface bilayer lipid membrane dimensions *Langmuir* **27** 618–26
[48] Rizzi F, Qualtieri A, Dattoma T, Epifani G and De Vittorio M 2015 Biomimetics of underwater hair cell sensing *Microelectron. Eng.* **132** 90–7
[49] Robles L and Ruggero M A 2001 Mechanics of the Mammalian Cochlea *Physiol. Rev.* **81** 1305–52
[50] Sapra K T and Bayley H 2012 Lipid-coated hydrogel shapes as components of electrical circuits and mechanical devices *Sci. Rep.* **2**
[51] Sarles S A 2013 The use of virtual ground to control transmembrane voltages and measure bilayer currents in serial arrays of droplet interface bilayers *Smart Mater. Struct.* **22** 094023
[52] Sarles S A and Leo D J 2009 Tailored current—voltage relationships of droplet-interface bilayers using biomolecules and external feedback control *J. Intell. Mater. Syst. Struct.* **20** 1233–47
[53] Sarles S A and Leo D J 2010 Physical encapsulation of droplet interface bilayers for durable, portable biomolecular networks *Lab Chip* **10** 710–7
[54] Sarles S A and Leo D J 2010 Regulated attachment method for reconstituting lipid bilayers of prescribed size within flexible substrates *Anal. Chem.* **82** 959–66
[55] Sarles S A, Madden J D and Leo D J 2011 Hair cell inspired mechanotransduction with a gel-supported, artificial lipid membrane *Soft Matter* **7** 4644–53
[56] Sarles S A, Stiltner L J, Williams C B and Leo D J 2010 Bilayer Formation between lipid-encased hydrogels contained in solid substrates *ACS Appl. Mater. Interfaces* **2** 3654–63
[57] Schroeder T B, Bruhn B R, Li S, Billeh Y N, Wang K and Mayer M 2014 Dynamics of bio-inspired pressure generation *Biophys. J.* **106** 615
[58] Stokes G G 1851 On the effect of the internal friction of fluids on the motion of pendulums *Trans. Camb. Phil. Soc.* **9** 8–106
[59] Sukharev S I, Blount P, Martinac B, Blattner F R and Kung C 1994 A large-conductance mechanosensitive channel in *E. coli* encoded by mscL alone *Nature* **368** 265–8
[60] Syeda R, Holden M A, Hwang W L and Bayley H 2008 Screening blockers against a potassium channel with a droplet interface bilayer array *J. Am. Chem. Soc.* **130** 15543–8
[61] Tamaddoni N, Freeman E C and Sarles S A 2015 Sensitivity and directionality of lipid bilayer mechanotransduction studied using a revised, highly durable membrane-based hair cell sensor *Smart Mater. Struct.* **24** 065014
[62] Tamaddoni N, Taylor G J, Hepburn T, Kilbey M and Sarles S A 2016 Reversible, voltage-activated formation of biomimetic membranes between triblock copolymer-coated aqueous droplets in good solvents *Soft Matter* submitted
[63] Taylor G J, Venkatesan G A, Collier C P and Sarles S A 2015 Direct in situ measurement of specific capacitance, monolayer tension, and bilayer tension in a droplet interface bilayer *Soft Matter* **11** 7592–605
[64] Villar G, Graham A D and Bayley H 2013 A tissue-like printed material *Science* **340** 48–52
[65] Villar G, Heron A J and Bayley H 2011 Formation of droplet networks that function in aqueous environments *Nat. Nano* **6** 803–8
[66] Wauer T, Gerlach H, Mantri S, Hill J, Bayley H and Sapra K T 2013 Construction and manipulation of functional three-dimensional droplet networks *ACS Nano* **8** 771–9
[67] Wong D, Jeon T-J and Schmidt J 2006 Single molecule measurements of channel proteins incorporated into biomimetic polymer membranes *Nanotechnology* **17** 3710
[68] Yang Y, Nguyen N, Chen N, Lockwood M, Tucker C, Hu H, Bleckmann H, Liu C and Jones D L 2010 Artificial lateral line with biomimetic neuromasts to emulate fish sensing *Bioinsp. Biomim.* **5** 016001